REDUCING THE IMPACT OF METAL IMPURITIES IN BLOCK-CAST MC SILICON

J. Junge, A. Herguth, S. Seren, G. Hahn
University of Konstanz, Department of Physics, P.O. Box X916, 78457 Konstanz, Germany
Author for correspondence: Johannes.Junge@uni-konstanz.de, Tel.: +49 7531 88 2082, Fax: +49 7531 88 3895

ABSTRACT: The detrimental influence of transition metals on minority carrier lifetime in solar cells and thus solar cell performance is up to now not fully understood. In this paper we would like to contribute some new results on this topic concerning the gettering and deactivation of the transition metals iron (Fe) and copper (Cu) in block cast multicrystalline (mc) Si material. The investigated processing steps include extended $POCl_3$ gettering and hydrogenation by firing of a PECVD (Plasma-Enhanced Chemical Vapor Deposition) silicon nitride (SiN_x:H). They are carried out on neighboring wafers using processing conditions which are derived from the standard photolithography based process at the University of Konstanz (UKN). Sets of neighboring wafers are selected from bottom, middle and top of an ingot, respectively, to address the varying impurity concentrations e.g. due to segregation during ingot casting. To extract the specific influence of the transition metals, wafers from intentionally contaminated mc material were examined. Hydrogenation clearly turned out to have the biggest positive influence on the contaminated material, while extended gettering showed non-uniform results. In some cases an improvement was observed, but also degradation of the bulk material occurred.
Keywords: mc-Si, impurities, hydrogenation, gettering

1 INTRODUCTION

In order to reduce the costs of silicon wafers for solar cell production one way is to use less purified raw material. In most cases this leads to reduced solar cell performance but the detailed correlation of impurity concentration and performance level of the solar cell is not yet fully understood. In this paper we focus on the impact of transition metal impurities (Fe and Cu) on the bulk of the solar cell. Therefore different solar cell processing schemes are applied to mc-wafers originating from intentionally contaminated ingot material. The processing steps under investigation include an extended gettering step after the standard $POCl_3$ emitter diffusion and hydrogen passivation during firing of a PECVD SiN_x:H layer at high temperatures as well as the combination of both steps - extended gettering and hydrogenation.

2 INVESTIGATED MATERIALS

The investigated materials were taken from several ingots which were fabricated within the SolarFocus project [1]. Table I gives an overview over all ingots fabricated to address this matter. Material from all ingots except ingot 4 was taken and underwent the different processing steps described below. More details about the material investigated here can be found in [2].

Table I: Overview of the six cast ingots with additional Fe/Cu contamination in the melt. Ingot 4 was not investigated in this work.

Ingot number	Additional metallic impurity
(1)	0 ppma Fe + 0 ppma Cu
(2)	2 ppma Fe + 0 ppma Cu
(3)	20 ppma Fe + 0 ppma Cu
(4)	0 ppma Fe + 20 ppma Cu
(5)	2 ppma Fe + 20 ppma Cu
(6)	20 ppma Fe + 20 ppma Cu

3 PROCESSES

To ensure a good comparability between the four different processing schemes A, B, C and D depicted in Figure 1, they are performed on neighboring wafers, respectively. At first all wafers (standard thickness of 250 µm) are cut from 12.5x12.5 cm^2 or 15.6x15.6 cm^2 wafers to a size of 5x5 cm^2 to fit the requirements of the photolithography equipment at UKN. The next step is a polishing etch consisting of HF, HNO_3 and CH_3COOH to remove the saw damage. $POCl_3$ emitter diffusion is carried out in a conventional open tube diffusion furnace. For processes C and D this step is prolonged with a temperature plateau of 1 hour at 700°C to enhance the $POCl_3$ gettering effect. After that, wafers from processes A and C receive a hydrogen-rich PECVD silicon nitride layer (SiN_x:H) as antireflection coating and for hydrogenation during Al-BSF formation. To prevent unintentional hydrogen passivation during the PECVD deposition [3] this step is omitted in the processes B and D. To form an Al-BSF a conventional Al metallization paste is screenprinted on the backside of all wafers then dried and fired in a conventional belt furnace. This step also releases hydrogen from the SiN_x:H layer for the high temperature hydrogenation. After wet chemical etching of the Al paste, the front contacts are defined either by photolithography and evaporation of Ti, Pd and Ag (processes A and C) followed by Ag plating or by simple evaporation of the metals through a shadow mask (processes B and D) without Ag plating. Al for the rear contact is also evaporated. Finally four solar cells (format 2x2 cm^2) are cut out of each 5x5 cm^2 wafer with a dicing saw. A contact sintering step finalizes the process.

As it is well known that impurities are not distributed homogeneously over the whole ingot during crystallization [4, 5], sets of wafers are taken from the lowest bottom region, the middle and the highest top region of the ingot to address the varying iron and copper concentration over the ingot height.

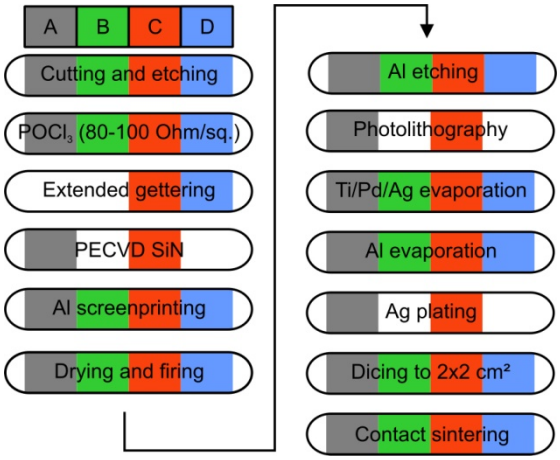

Figure 1: Process flowchart depicting the four different processes A, B, C and D.

4 CHARACTERIZATION

As the different processing schemes shown in figure 1 lead to different cell layouts (different front grid, front surface with or without SiN_x antireflection layer (ARC)), the best way to compare the bulk material of cells from all four schemes is the Internal Quantum Efficiency (IQE). Nonetheless, standard IV-measurements were also carried out to check the reliability of the process (indicated by a high fill factor). LBIC scans were performed as well to see the influence of the different processing schemes on grain boundaries.

5 NAA AND IQE RESULTS

Results for the four different processing schemes on wafers from the bottom, middle and top of the respective ingot are depicted in the following subsections. The first graph gives an overview over the iron and copper distribution over the ingot height as well as the exact positions of the processed wafers which are later on only referred to as 'bottom', 'middle' and 'top' of the ingot. The Fe and Cu distributions were obtained by Neutron Activation Analyses (NAA) within the SolarFocus project. Data of the reference ingot is given in figure 2. The IQE curves of wafers processed according to scheme B and D all show reduced IQE in the short wavelength regime which is due to the lacking front surface passivation. To determine the quality of the bulk material concerning bulk defect engineering, however, this is of minor relevance. Thus, only the long wavelength IQE between 800 nm and 1100 nm is depicted in the following subsections.

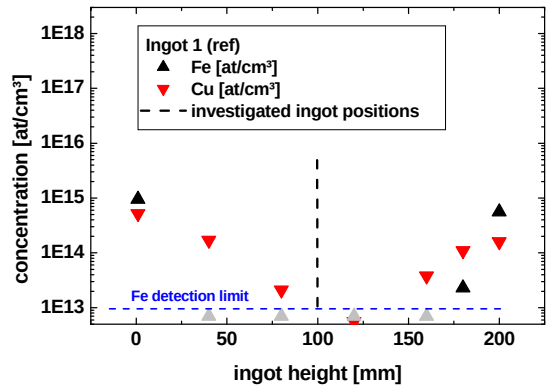

Figure 2: Fe and Cu concentration over the ingot height of the reference ingot (ingot 1). Fe concentration was below the detection limit in the middle of the ingot (grey symbols). The dashed line indicates the origin of the processed reference wafers.

5.1 Ingot 2 (additional 2 ppma Fe)

Figure 3 depicts the Fe and Cu distribution over the ingot height of ingot 2. Wafers were taken from 18% ingot height (34 mm; 'bottom'), 50% ingot height (100 mm; 'middle') and 90% ingot height (180 mm; 'top'), respectively.

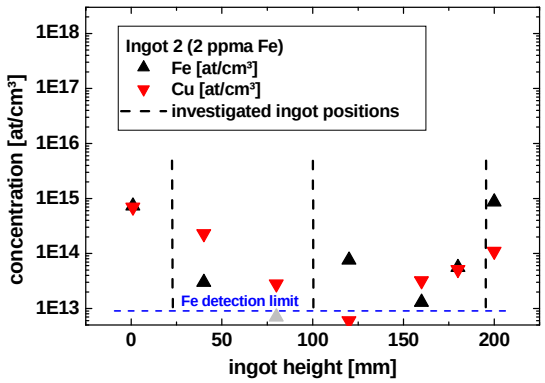

Figure 3: Fe and Cu concentration over the ingot height (ingot 2). Fe concentration was below the detection limit in the middle of the ingot (grey symbol). Dashed lines indicate the origin of the processed wafers.

In addition to the information about the height it should be mentioned that for this ingot the processed 5x5 cm² wafers were taken close to the edge of the ingot and are therefore more affected by impurities originating from the crucible walls.

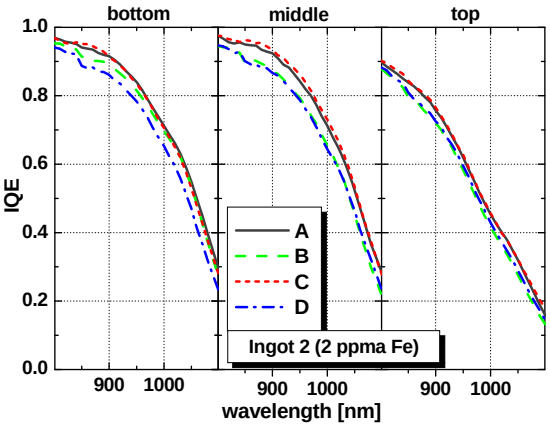

Figure 4: IQE characterization of ingot 2 (800-1100 nm, same scaling). Curves show IQE measurements of 4 neighboring cells from bottom, middle and top, respectively, which underwent the different processing schemes.

Results for the four different processing schemes on wafers from the bottom, middle and top of ingot 2 are

depicted in figure 4. Cells from all three parts of the ingot benefit from the high temperature hydrogenation (processes A and C). Extended gettering, however, does not show a uniform behavior. In most cases it does not seem to influence the IQE at all. Only in combination with the hydrogenation a slight improvement is visible on the cell from the middle of the ingot. For the cell from the bottom region without hydrogenation by contrast it seems to have even a detrimental influence.

5.2 Ingot 3 (additional 20 ppma Fe)

Figure 5 depicts the iron and copper distribution over the ingot height of ingot 3. Wafers were taken from 4% ingot height (8 mm; 'bottom'), 50% ingot height (100 mm; 'middle') and 92% ingot height (183 mm; 'top') respectively.

Although the only intentional contamination consists of Fe, the Cu content of this ingot is unusually high compared to the reference block. This might be explained by an unintentional contamination during ingot casting, which cannot be ruled out completely.

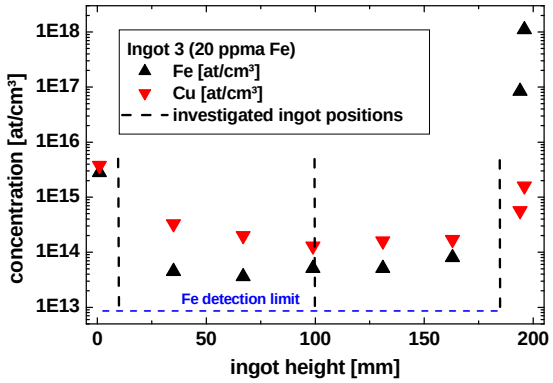

Figure 5: Fe and Cu concentration over the ingot height (ingot 3). Dashed lines indicate the origin of the processed wafers.

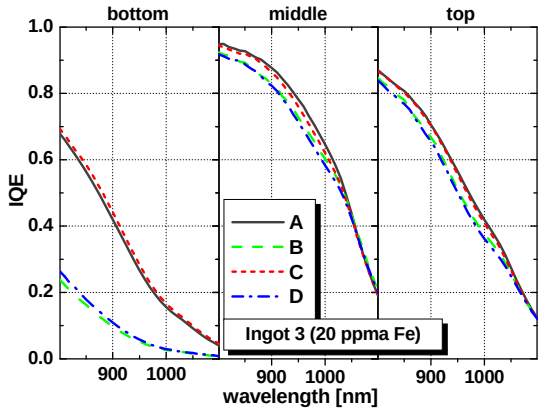

Figure 6: IQE characterization of ingot 3 (800-1100 nm, same scaling). Curves show IQE measurements of 4 neighboring cells from bottom, middle and top, respectively, which underwent the different processing schemes.

For the bottom region it is clearly visible that extended gettering enhances the long wavelength IQE and so the bulk quality. Also the hydrogen from the SiN_x:H has the biggest influence in the bottom region of the ingot. For the middle and top of the ingot, extended gettering shows no beneficial influence (the tendency appears to be even negative). Hydrogenation, however, has a positive effect also in these regions (figure 6).

5.3 Ingot 5 (additional 2 ppma Fe and 20 ppma Cu)

Figure 7 depicts the Fe and Cu distribution over the ingot height of ingot 5. Wafers were taken from 18% ingot height (34 mm; 'bottom'), 50% ingot height (100 mm; 'middle') and 95% ingot height (190 mm; 'top'), respectively.

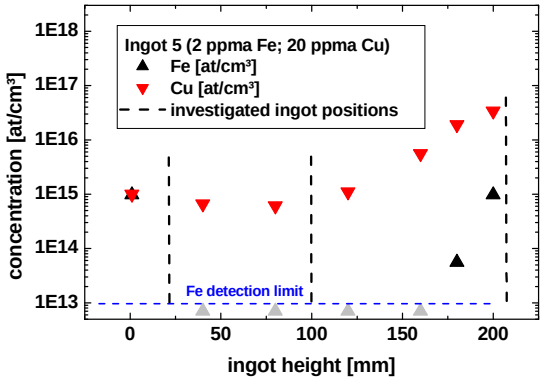

Figure 7: Fe and Cu concentration over the ingot height (ingot 5). Fe concentration was below the detection limit in the middle of the ingot (grey symbols). Dashed lines indicate the origin of the processed wafers.

In addition to the information about the height it should be mentioned that for this ingot the processed 5x5 cm² wafers were taken from the edge of the ingot and are therefore more affected by impurities originating from the crucible walls.

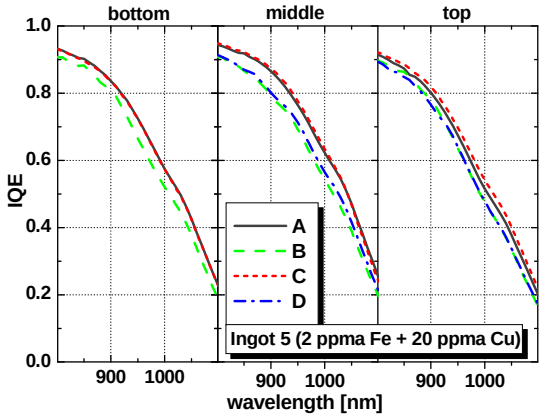

Figure 8: IQE characterization of ingot 5. Curves show IQE measurements (800-1100 nm, same scaling) of neighboring cells from bottom, middle and top, respectively, which underwent the different processing schemes. The wafer of the bottom region processed according to process D broke during processing.

Figure 8 depicts as already observed before the beneficial influence of the hydrogenation in all regions of the ingot. Extended gettering this time has only a small beneficial effect combined with the hydrogenation in the top region (process C) and without hydrogenation in the middle of the ingot (process D). In all other cases no influence is detectable. Due to breakage process D could not be evaluated in the bottom region of this ingot.

5.4. Ingot 6 (additional 20 ppma Fe and 20 ppma Cu)

Figure 9 depicts the Fe and Cu distribution over the ingot height of ingot 6. Wafers were taken from 4% ingot height (8 mm; 'bottom'), 50% ingot height (100 mm; 'middle') and 91% ingot height (181 mm; 'top') respectively.

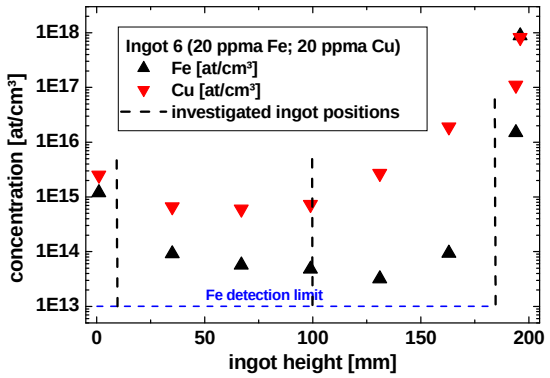

Figure 9: Fe and Cu concentration over the ingot height (ingot 6). Dashed lines indicate the origin of the processed wafers.

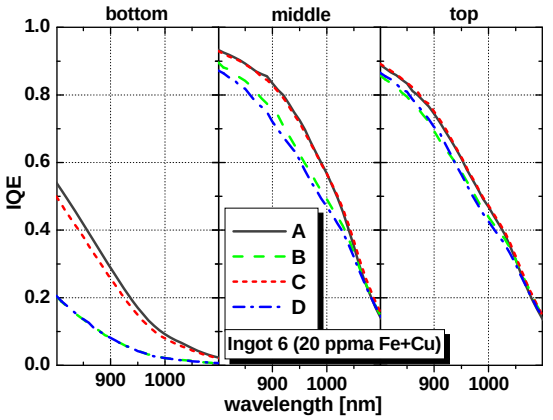

Figure 10: IQE characterization of ingot 6. Curves show IQE measurements (800-1100 nm, same scaling) of 4 neighboring cells from bottom, middle and top, respectively, which underwent the different processing schemes.

Figure 10 shows the long wavelength IQE data obtained from cells of ingot 6. Hydrogenation again shows the biggest beneficial effect in every region of the ingot. Extended gettering has no positive effect. In some cases (process C in the bottom region and process D in the middle of the ingot) it even tends to decrease the IQE.

6 IV CHARACTERISATION

Though not the primary focus of the investigations presented here, the initial purpose of process A, from which all other processes are derived, is the determination of efficiency limits of mc silicon materials. Applying that process, for ingot 3 (additional 20 ppma Fe) well above 16% efficiency were achieved in the middle of the ingot (table II). This even slightly exceeds the results obtained on the reference material. The data supports observations of G. Coletti et al. for industrial-type processing, who experienced only minor efficiency drawbacks on material even higher contaminated with Fe [6]. In contrast to our expectations, for process C there was no efficiency gain observed (table III). However, this matches with the IQE data from above.

Table II: IV characteristics of solar cells processed according to process A. Cells originate from the reference ingot as well as from bottom, middle and top of ingot 3.

ingot	FF [%]	J_{sc} [mA/cm²]	V_{oc} [mV]	η [%]	Δη [%]
(1) Ref.	78.5	32.3	618	15.7	0
(3) Bottom	77.6	26	587	11.9	-24.2
(3) Middle	80.3	32.5	628	16.4	4.5
(3) Top	75.5	29.8	606	13.6	-13.4

Table III: IV characteristics of solar cells processed according to process C. Cells originate from the reference ingot as well as from bottom, middle and top of ingot 3.

ingot	FF [%]	J_{sc} [mA/cm²]	V_{oc} [mV]	η [%]	Δη [%]
(1) Ref.	79	33.1	618	16.1	0
(3) Bottom	78.5	26.1	588	12.1	-24.8
(3) Middle	79.7	32.2	624	16	-0.6
(3) Top	58.5	29.5	589	10.2	-36.6

IV-data from solar cells originating from ingot 6 is given in table IV and V. 15% efficiency was exceeded for wafers from the middle of the ingot. Process C, however, does not show a significant improvement compared to process A as already shown for ingot 3.

Table IV: IV characteristics of solar cells processed according to process A. Cells originate from the reference ingot as well as from bottom, middle and top of ingot 6.

ingot	FF [%]	J_{sc} [mA/cm²]	V_{oc} [mV]	η [%]	Δη [%]
(1) Ref.	78.5	32.3	618	15.7	0
(6) Bottom	78	22.8	565	10.1	-35.7
(6) Middle	79.4	31	611	15	-4.5
(6) Top	78.1	29.8	604	14.1	-10.2

Table V: IV characteristics of solar cells processed according to process C. Cells originate from the reference ingot as well as from bottom, middle and top of ingot 6.

ingot	FF [%]	J_{sc} [mA/cm²]	V_{oc} [mV]	η [%]	Δη [%]
(1) Ref.	79	33.1	618	16.1	0
(6) Bottom	78.3	22	558	9.6	-40.4
(6) Middle	80.1	31.1	610	15.2	-5.6
(6) Top	79.4	29.9	606	14.4	-10.6

For correct interpretation of the IV data it should be added that all cells were neither textured nor was the ARC layer thickness at an optimum (minimum of reflectance at 540 nm). From this point of view it is astonishing how high the efficiency potential even of the highly contaminated material is. Especially a V_{oc} of 628 mV (middle of ingot 3) is unusually high even for very pure mc silicon material.

7 INFLUENCE ON GRAIN BOUNDARIES

To investigate the recombination activity of the grain boundaries regarding the four different processing schemes, high resolution LBIC measurements were carried out. Figure 11 shows LBIC maps of the same area on the four different solar cells processed according to process A, B, C and D, respectively. While the extended gettering (C and D) does not show deviations compared to the standard gettering (A and B), a clear influence of the hydrogenation via SiN_x:H is visible. Some grain boundaries which are clearly visible (highly recombination active) on the samples from processes B and D are almost completely deactivated in the hydrogenated samples (A and C). Interestingly not all grain boundaries behave the same way. This leads to the assumption that decoration and/or type of the grain boundary play a major role concerning the possibility of passivation during hydrogenation. Similar effects were recently observed on pure mc material ('mc-FZ') [7].

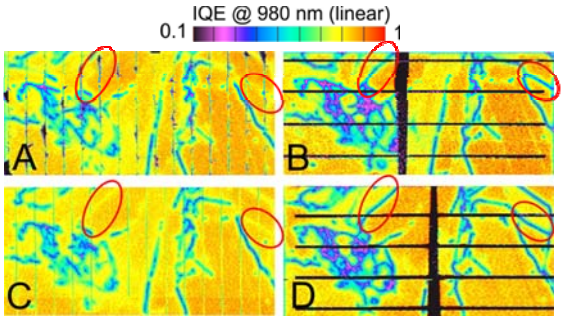

Figure 11: LBIC measurement of neighboring cells from the bottom of ingot 2 which underwent the different processing schemes (mapped area: 17x8 mm^2).

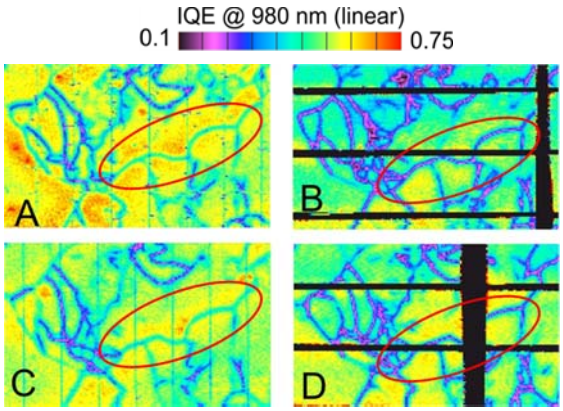

Figure 12: LBIC measurement of neighboring cells from the top of ingot 2 which underwent the different processing schemes (mapped area: 8x5 mm^2).

Figure 12 shows LBIC scans from the top of ingot 2. The behavior of the grain boundaries is similar to the observation made at the bottom of the ingot, though the grain boundaries are no longer completely passivated. This indicates that there is a certain concentration limit for impurities which can be passivated (after a gettering step) via high temperature hydrogenation. This limit seems to be exceeded in the top region (90% height) of this ingot due to segregation effects.

8 CONCLUSION

High temperature hydrogenation by firing of a hydrogen-rich PECVD-SiN_x:H turns out to be the most important tool to improve the bulk quality of Si-material containing large amounts of Fe and Cu. So it might be appropriate to optimize the SiN_x:H layer for solar cells from heavier contaminated ingot material not only regarding the antireflection behavior and the firing of the front contacts, but also concerning the hydrogen passivation during the firing of the front contacts. Regarding extended gettering (1 additional hour at 700°C) no reliable conclusion can be drawn. In some cases a small beneficial effect was observed, especially in combination with the hydrogenation. But in most cases the effect was too small to be detected by means of IQE measurements and sometimes even a decreased IQE was observed for the processes containing the extended gettering step.

However, it has to be mentioned that dealing with defects and impurities in mc Si material is a rather complex matter, as it is impossible to study one type of defect or impurity on its own. Additionally, the investigations presented in this study lack a better statistical validation. Nevertheless, first general trends and effects of the various impurity concentrations on cell parameters could be shown. So there is still a lot of work ahead to get a better view of the whole picture.

9 OUTLOOK

Further investigations on this material will address the detailed analysis of the grain boundaries as gettering sites and the comparison of contact sintering with and without an atomic hydrogen ambient. In addition, microscopic analysis will be performed in parallel to investigate the interactions between impurities and extended lattice defects.

10 ACKNOWLEDGEMENTS

The underlying project of this report was financially supported by the German Federal Ministry for the Environment, Nature Conservation and Nuclear Safety within the research cluster SolarFocus (0327650H) and all the industry partners.The financial support from the BMU project 0325079 is also gratefully acknowledged, in particular for the processing and characterization equipment. The NAA results were provided by the coordination of the SolarFocus project. We would also like to thank Bärbel Rettenmaier, Lisa Rothengaß, Annika Zuschlag, Sarah Gindner and Joachim Ruck for support during processing. The content of this publication is the responsibility of the authors.

11 REFERENCES

[1] S. Riepe, I.E. Reis, W. Koch, "Solar silicon material research network SolarFocus (Solarsilizium Forschungscluster)," *Proc. 23rd EU-PVSEC*, Valencia 2008, p 1410.

[2] I.E. Reis, S. Riepe, and W. Koch, "Effect of impurities on solar cell parameters in intentionally contaminated multicrystalline silicon," *Proc. 24th EU-PVSEC*, Hamburg 2009.

[3] B. Herzog, G. Hahn, M. Hofmann, I.G. Romijn, A.W. Weeber, "Bulk hydrogenation in mc-si by PECVD SiN_x deposition using direct and remote plasma", *Proc. 23rd EU-PVSEC*, Valencia 2008, p. 1863.

[4] K. Lauer, M. Ghosh, A. Lawerenz, S. Dauwe, "Minority carrier lifetime, trap density and interstitial iron content in multicrystalline silicon raw wafers versus ingot position", *Proc. 21st EU-PVSEC*, Dresden 2006, p. 1362.

[5] R. Kvande, L.J. Geerligs, G. Coletti, L. Arnberg, M. Di Sabatino, E.J. Ovrelid, and C.C. Swanson, "Distribution of iron in multicrystalline silicon ingots", *Journal of Applied Physics*, 2008, vol. 104, p. 064905-9.

[6] G. Coletti, R. Kvande, V.D. Mihailetchi, L.J. Geerligs, L. Arnberg, and E.J. Ovrelid, "Effect of iron in silicon feedstock on p- and n-type multicrystalline silicon solar cells", *Journal of Applied Physics*, 2008, vol. 104, p. 104913-11.

[7] A. Zuschlag, G. Micard, J. Junge, M. Käs, S. Seren, G. Hahn, G. Coletti, G. Jia, W. Seifert, "Investigations on the recombination activity of grain boundaries in mc silicon," *33rd IEEE Photovoltaic Specialists Conference*, San Diego, 454, 2008.